applied sciences

MDPI

Article

Defining Robust NVH Requirements for an Electrified Powertrain Mounting System Based on Solution Space During Early Phase of Development

José G. Cóndor López [1,*], Karsten Finger [1] and Sven Herold [2]

[1] Mercedes-Benz AG, 71059 Sindelfingen, Germany; karsten.finger@mercedes-benz.com
[2] Fraunhofer Institute for Structural Durability and System Reliability LBF, 64289 Darmstadt, Germany; sven.herold@lbf.fraunhofer.de
* Correspondence: jose_gabriel.condor_lopez@mercedes-benz.com

Abstract

Electrification introduces additional NVH (noise, vibration and harshness) challenges during the development of powertrain mounting systems due to high-frequency excitations from the powertrain and the absence of masking effects from the combustion engine. In these frequency ranges, engine mounts can stiffen up to a factor of five due to continuum resonances, reducing their structure-borne sound isolation properties and negatively impacting the customer's NVH perception. Common hardening factors used during elastomer mount development are therefore limited in terms of their applicable validation frequency range. This study presents a methodology for determining decoupled permissible stiffness ranges for a double-isolated mounting system up to 1500 Hz, based on solution space engineering. Instead of optimizing for a single best design, we seek to maximize solution boxes, resulting in robust stiffness ranges that ensure the fulfillment of the formulated system requirements. These ranges serve as NVH requirements at the component level, derived from the sound pressure level at the seat location. They provide tailored guidelines for mount development, such as geometric design or optimal resonance placement, while simultaneously offering maximum flexibility by spanning the solution space. The integration of machine learning approaches enables the application of large-scale finite-element models within the framework of solution space analysis by reducing the computational time by a factor of $7.19 \cdot 10^3$. From a design process standpoint, this facilitates frontloading by accelerating the evaluation phase as suppliers can directly benchmark their mounting concepts against the permissible ranges and immediately verify compliance with the defined targets.

Keywords: NVH; powertrain integration; SSE; mounting system; BEV; finite-element simulation; data-driven model; dynamic stiffness; early phase

check for updates

Academic Editor: Junhong Park

Received: 29 July 2025
Revised: 14 September 2025
Accepted: 17 September 2025
Published: 20 September 2025

Citation: Cóndor López, J.G.; Finger, K.; Herold, S. Defining Robust NVH Requirements for an Electrified Powertrain Mounting System Based on Solution Space During Early Phase of Development. *Appl. Sci.* **2025**, *15*, 10241. https://doi.org/10.3390/app151810241

Copyright: © 2025 by the authors. Licensee MDPI, Basel, Switzerland. This article is an open access article distributed under the terms and conditions of the Creative Commons Attribution (CC BY) license (https://creativecommons.org/licenses/by/4.0/).

1. Introduction

The development of battery electric vehicles (BEVs) is characterized by novel requirements regarding acoustic comfort due to the fundamentally different acoustical behavior of their electrified powertrains resulting in high-frequency excitation spectra in comparison to internal combustion engines [1,2]. In this context, vehicle acoustics, as measured by the interior noise level within the cabin, serve as an indicator of the perceived quality impression and consequently the customer acceptance of BEVs [1]. Moreover, more than 50% of customer complaints relate to different components that emit specific electric noise,

which is coming to the fore due to the absence of masking effects, specially at lower driving speeds [3,4]. The highest rates of functional noise complaints are related to the powertrain [5]. The high-pitched tonal noise emitted by the powertrain is characterized by a high frequency range of up to 10 kHz and single-tonality components. At these frequency ranges, human hearing is especially sensitive and therefore readily perceivable even at low sound pressure levels [3,6–9]. The main noise sources consist of the electric motor, power electronics and geartrain within the electric powertrain [2,3].

In order to fulfill these novel requirements, heavy corrective measures, e.g., a mass-damper or heavy layers, are usually integrated into the vehicle, which at the same time conflict with other discipline targets such as efficiency. Especially at late development stages, this insertion is crucial and cannot be compensated by other components in the sense of weight reduction, resulting in a degradation in the electric range. Furthermore, there is a growing number of lightweight approaches introduced in modern vehicles with the aim of enlarging the driving range. These concepts are more prone to vibration and therefore unfavorable for acoustics [2]. In addition, in the development of the electric axle, which is characterized by strong coupling between the powertrain and chassis, the well-established and proven methods during development and extensive experience from former axle systems need to be extended [10]. These new challenges have to be addressed at early stages of the development process in order to define a suitable powertrain mounting system (PMS) regarding NVH. Especially, coupling elements, e.g., engine mounts or subframe mounts, which are critically important for the transmission of vibration and structure-borne noise from the powertrain to the vehicle interior [9], represent in this context significant potential for improvement by specifically adapting isolation properties or compensating for structural weaknesses of the PMS [9–11]. Nevertheless, the isolation performance of engine mounts is constrained in the high frequency range due to the presence of the mount continuum resonances, resulting in significant stiffening effects and amplifying the structure-borne noise towards interior cabin [8,9,11]. Consequently, this high-frequency transfer behavior of the mounts must be accounted for during the early phases of development to prevent the superposition of resonances along the transmission path or to position them in non-critical frequency bands where low excitation levels from the drive unit occur [11]. On the other hand, conventional simulation approaches relying on static stiffnesses are only valid within the low frequency range [9]. Approaches for the targeted modification of mount transfer behavior have been reported in the literature. In [11] a topology optimization of an elastomeric mount is proposed with the aim of improving the high-frequency transfer behavior up to 2 kHz. Similarly, Ref. [12] shows that both metamaterials and geometric features on top of the rubber can effectively manipulate the continuum resonances of the mounts within the high frequency range. The early design phase enables major flexibility regarding shaping of the engine mount such as the geometrical features, number of mounts or mount layout [13]; on the other hand, this phase is characterized by uncertain and imprecise data [14]. Therefore, one of the primary objectives during the concept phase of the mounting system is to generate robust solutions with respect to flexibility for later changes in design and the increasing maturity of vehicle data [13]. In order to handle the uncertainty of complex systems, set-based design approaches provide uncertainty consideration as well as flexibility for the choice of design variables in comparison to point-based methods [15]. Solution space engineering (SSE) represents a set-based design approach, first introduced by [16], and seeks to identify regions in the design space by numerical sampling where all system requirements are fulfilled, the so-called solution space. By constraining the solution space to box-shaped regions, known as a solution box, the design variables are fully decoupled and can be adjusted independently without violating any requirements. Automotive application fields of SSE

referring to PMSs are presented in [17], which proposes an interdisciplinary engine mount design process that considers different development disciplines for the static stiffness and low-frequency mount behavior. In [13], the SSE approach is employed to derive static curves of a conventional PMS, modeled using a power function parameterized by nine variables in each spatial direction, resulting in a high-dimensional optimization problem. The first approach to identifying the isolation properties of an elastomeric mount for an electric compressor in high frequency ranges up to 1 kHz is presented in [18]. Using Dynamic Substructuring and transfer path analysis, the method quantifies admissible stiffness ranges as circular solution spaces for each element, demonstrated on an electric compressor in a vehicle. In [19], the challenge of accurately defining vibration requirements for electric motors is addressed and demonstrated through an analytical example. In particular, when electric motors or components are outsourced to suppliers, field experience indicates that even if components meet the predefined requirements, the full vehicle may still exhibit unacceptable noise levels [20]. Moreover, the definition of targets are mandatory for clear division of responsibilities in this context [19].

This work presents a design procedure for identifying robust NVH requirements for engine mounts of an electric PMS using the set-based design approach SSE. The frequency range up to 1.5 kHz is discretized, allowing for an identification of a solution box at each frequency band. By allocating these solution-boxes across the frequency range, a frequency-dependent permissible interval for each design variable is generated.

This study expands the application field of solution space engineering to the identification of mount isolation properties of a mounting systems for electric drive units, considering a wider frequency range due to the presence of continuum resonances in engine mounts. Moreover, this study enables the application of large-scale finite-element models within the framework of solution space analysis by incorporating machine learning models to reduce numerical effort.

2. Methodology and Workflow

In this section, the development approach for defining robust NVH requirements for an electrified PMS is presented. The methodologies used, as well as the proposed workflow, are briefly explained.

2.1. Electric Powertrain Mounting System

In Figure 1 a double decoupled mounting system of an electric drive unit (EDU), consisting of a subframe as well as the first and second mount layers, is depicted. The corresponding mounts of each layer are also known as inner and outer mounts. While the inner mounts represent the decoupling layer between the EDU and the subframe, the second mounting layer connects the subframe to the vehicle body. In comparison to single-layer architectures, the double decoupled mounting system demonstrates superior isolation properties, especially in the high frequency range [21]. The mounting system considered in this work is adopted from a dedicated PMS architecture of an electric vehicle. The mounting topology consists of four inner mounts (inMs), with the rear ones rotated by 90° around the vertical z-axis, and four outer mounts, which are grouped into front outer mounts (foMs) and rear outer mounts (roMs). In the frequency domain, each mount is described functionally by its translational and rotational stiffness, as well as their corresponding phase information.

In the following, only the structure-borne noise path through the mounting system into the interior cabin is considered. Additional structure-borne noise paths, such as sideshafts or high-voltage cables, as well as airborne noise radiation of the EDU, are not within the scope of this work.

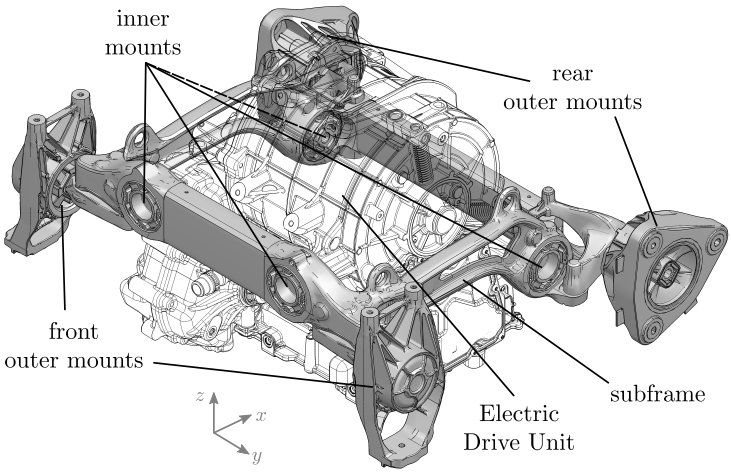


Figure 1. Double-decoupled PMS consisting of an EDU, a subframe and first and second mount layers.

2.2. Workflow

The overall workflow for defining robust NVH requirements for the mounting system is illustrated in Figure 2. In the first step, the mount parameters to be determined are defined and serve as input for the training data of data-driven models in order to reduce numerical effort. For an evenly distributed sample point allocation within the design space, we use the Latin Hypercube Sampling method. Depending on the number of parameters and system complexity, the number of sample points can vary. In this work, we propose an initial setup of 1000 data points x_p. If the resolution of the design space by the sample points is insufficient, the number of sample points is increased iteratively. This evaluation takes place during the training phase of the data-driven model.

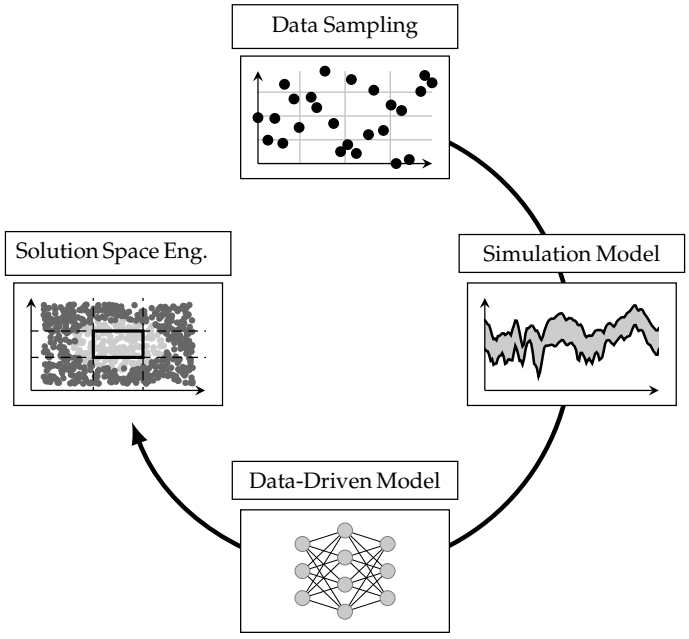


Figure 2. Schematic workflow for defining robust NVH requirements of mount characteristics using data-driven models and SSE, resulting in a frequency-dependent permissible range for each mount.

In the next step, the generated data points are forwarded to the simulation model, which calculates the forces at the outer mounts for a predefined loadcase. For the calculation of the target quantity, the sound pressure level (SPL) inside the cabin, we use a hybrid modeling technique that combines simulation with measured vehicle transfer functions. The frequency range of interest is between 250 and 1500 Hz.

To improve numerical performance in terms of time cost per function evaluation, data-driven models based on Neural Networks (NNs) are introduced. They act as regression models, mapping the input mount parameters to SPL at the driver's seat for the given frequency range. The calculation of such a data model represents the third step.

The last step is defined by the solution space analysis and the generation of a solution box for the mount parameters fulfilling the formulated requirements at each frequency. Concatenating the solution boxes over the entire frequency range results in a frequency-dependent permissible range for each mount parameter.

2.3. Simulation Model

The simulation model used in this work corresponds to a hybrid modeling approach for the calculation of structure-borne induced SPL inside the cabin. In order to adequately cover the frequency range of interest, more accurate finite-element (FE) models of the powertrain are required [22], which leads to larger simulation time. The powertrain components, composed of the electric motor, gear stages, housing and mount brackets as well as the subframe, are fully represented by three-dimensional FEs such as 10-node quadratic tetrahedral elements. The sideshafts are modeled as three-dimensional beam elements in order to capture axial and bending behavior. Fixed boundary conditions, i.e., zero displacement and zero rotation, were applied at the sideshaft outer joints as well as the outer mounts on the vehicle side. This study focuses on gear whining loadcases. Therefore, excitation loads were applied as transmission error at the first gear stage between the two gear pairs. As a solver, we used `NxNastran` (version 2022.1).

Especially for the frequency range of interest, the material hardening as well as the continuum resonances of the mounts can lead to massive stiffening effects, causing degradation of isolation properties [21–23]. The consideration of stiffening effects is suitable as long as the mount characteristics are well known from high frequency measurements or simulations of the mount. For the exploration and generation of permissible stiffness intervals during the early phase of development, we propose a simple spring-damper modeling approach. The mount characteristics are therefore modeled by translational single-valued springs and damping factors for each direction over the entire frequency range. The stiffening effect of the mounts is considered implicitly by expanding the design space of the stiffness values by a factor of greater than two during the SSE analysis. In the following, we assume that the path through the mounts represents the major contributor to the overall structure-borne noise. Therefore, the structure-borne path through sideshafts is not further addressed in this study. Following, the sideshafts are rigidly mounted. In the case of a relevant contribution of the sideshaft, the axle must be taken into account.

The vehicle body side is represented by measured vehicle transfer functions, known as airborne-noise sensitivities. By multiplying the outer mount forces at the vehicle body coupling points with the transfer functions on the complex plane, we are able to calculate the SPL. This is performed for all translational degrees of freedom. As a target quantity, we choose the averaged SPL between the left and right microphone ear positions at the driver's seat. Acoustic quality criteria, such as the spatial distribution of noise or fluctuations, are beyond the scope of this study. Evaluation of these aspects could be addressed using full-vehicle simulation models rather than covering the vehicle side by measured data.

2.4. Data-Driven Model

Regarding numerical effort, the more accurate FE models as well as the considered frequency range force current high-performance computers to their limits [22]. Moreover, the direct usage of the FE model, as well as reduced models generated by modal reduction or the superelement technique provided by `NxNastran`, is still too time consuming for the

design space exploration by the SSE analysis. To overcome these limitations, data-driven models are introduced in order to approximate the system behavior accurate enough while reducing numerical effort. These models represent numerically efficient models in the sense of time evaluation and are feasible for high-dimensional optimization algorithms used by SSE.

In this work, NNs are considered as data-driven models due to their approximation capabilities to fit any function with a desired accuracy [24]. To predict the SPL $y_{\mathrm{spl}} \in \mathbb{R}^{f\times 1}$ given a mount characteristic $x_{\mathrm{p}} \in \mathbb{R}^{n\times 1}$, the function F_{nn} is described by

$$y_{\mathrm{spl}} = F_{\mathrm{nn}}\left(x_{\mathrm{p}}, p_{\mathrm{nn}}\right), \tag{1}$$

where p_{nn} denotes the weights and biases of the NN, f represents the frequency range of interest and n represents the number of mount parameters.

The architecture of the fully connected NN model used in this work consists of an input layer with x_{p} features, followed by three hidden layers with varying neuron sizes 2^9, 2^{10} and 2^9, respectively. Each hidden layer utilizes the Rectified Linear Unit (ReLU) as activation function to insert nonlinearities. The output layer consists of f neurons.

In this study, it was found that a batch size of 40, a learning rate of 0.1 and 4000 epochs provided sufficient model accuracy. As the optimization algorithm, we used Stochastic Gradient Descent to minimize the mean squared error (MSE), which is described by

$$\mathcal{L} = \frac{1}{k}\sum_i \mathcal{L}_i = \frac{1}{k}\sum_i \sum_j \left(y_{i,j} - \hat{y}_{i,j}\right)^2, \tag{2}$$

with the number of data points k, the training data $y_{i,j}$ and the prediction of the data-driven model $\hat{y}_{i,j}$. For the training phase, we allocated 80% of the data to train the model and reserved the remaining 20% for testing.

Besides the loss value, we used the coefficient of determination

$$R^2 = 1 - \frac{\sum_i \left(y_i - \hat{y}_i\right)^2}{\sum_i \left(y_i - \bar{y}\right)^2} \tag{3}$$

to measure the performance of the trained NN model [25]. Here, the actual value and its corresponding mean value are denoted by y_i and $\bar{y}$, respectively. The predicted value is presented by $\hat{y}_i$. While $R^2 = 1$ denotes a perfect prediction of the data by the model, $R^2 = 0$ indicates that the model does not predict the data better than the mean value.

The NN models were set up with the framework `PyTorch` (version 2.11) in the programming language `Python` (version 3.11).

2.5. Solution Space Engineering

The solution space engineering approach seeks to find a set of good solutions that fulfill all system requirements, rather than realizing a single point optimization. In this manner, a solution space is defined by [16] as

$$\Omega_{\mathrm{c}} := \{x \in \Omega_{\mathrm{ds}} \mid f(x) \leq f_{\mathrm{c}}\}, \tag{4}$$

where $\Omega_{\mathrm{ds}} \subset \mathbb{R}^d$ describes the design space, $f(x) \in \mathbb{R}^{m\times n}$ represents the evaluation function and $f_{\mathrm{c}} \in \mathbb{R}^m$ represents the set of system requirements that need to be fulfilled. This solution space can be arbitrarily shaped [13].

A solution box Ω_{sb} is a subset of the solution space, defined by the Cartesian product of permissible intervals I_i for each design variable x_i given as follows:

$$\Omega_{\mathrm{sb}} = \prod_{i=1}^{n} I_i = I_1 \times I_2 \times \ldots \times I_n. \tag{5}$$

Here, the interval $I_i = \left[x_i^{\mathrm{l}}, x_i^{\mathrm{u}}\right]$ is defined by two arbitrary design points with $x_i^{\mathrm{l}} \leq x_i^{\mathrm{u}}$, for $i = 1, \ldots, n$. The index l stands for lower, while the index u stands for upper. This leads to a complete decoupling, allowing each design variable to vary independently within its permissible range without violating any requirement. As a result, designers at the component level can act more independently for each component, which improves flexibility and accelerates the development process by reducing the number of iteration loops during distributed development [26].

In order to maximize the solution box within the solution space, a quantitative measure has to be introduced. Common measures in the literature are given by the n-dimensional volume or the size of the smallest interval [27]. In this work, the n-dimensional volume

$$\mu(\Omega) = \int_{\Omega} d\Omega \tag{6}$$

is considered.

However, increasing the dimensionality of the design space complicates the process of identifying solution boxes, and common visualization techniques are no longer practicable. For the purpose of this work, the visualization of a high-dimensional box-shaped solution space is based on the idea of projecting the solution box onto a two-dimensional plane that is defined by a pair of design variables x_{pair}. This idea is depicted in Figure 3 for a three-dimensional cubic design space, where the design space is projected onto the xz-plane. The evaluation function is the sphere function $x^2 + y^2 + z^2 = R^2$.

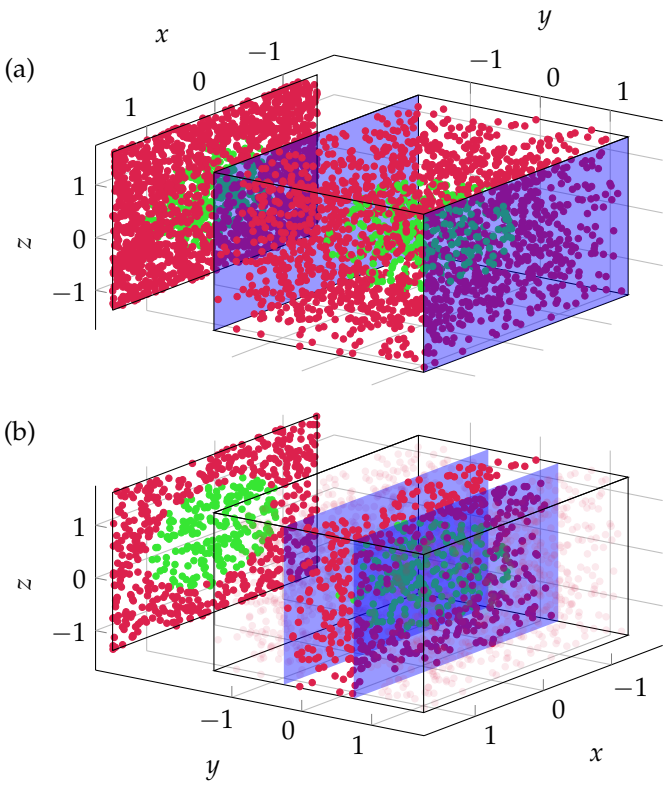


Figure 3. Projection technique of the SSE method on a three-dimensional design space: (**a**) projection of the entire interval I_y onto the xz-plane; (**b**) sliced design space in the y-direction. Green dots represent points inside the sphere, red dots outside.

In this case, the color green represents points inside the unit sphere while red points are located outside the sphere. At the top of Figure 3, the entire interval I_y is projected onto the xz-plane, resulting in indistinguishable solution areas on the plane. This subset concurrently represents the design space $\Omega_{\mathrm{ds}} = I_{\mathrm{x}} \times I_{\mathrm{y}} \times I_{\mathrm{z}}$. This is usually the first step in seeking a solution box. By slicing the design space of the design variable y, which means reducing the interval to $I_{\mathrm{y,red}}$, identifiable regions within the xz-plane become recognizable. The sliced design space is therefore described as $\Omega_{\mathrm{ds,red}} = I_{\mathrm{x}} \times I_{\mathrm{y,red}} \times I_{\mathrm{z}}$. This approach is also applicable for the remaining design variables x and z resulting in a box-shaped solution box.

A general formulation for a $n-2$-dimensional projection onto the pk-plane is given by

$$\Omega_{\mathrm{ds,red}} = I_{\mathrm{p}} \times I_{\mathrm{k}} \times \prod_{i=1, i \notin \{p,k\}}^{n} S_i, \tag{7}$$

where I_{p} and I_{p} denote the intervals of the design variables p and k, respectively. S_i represents a reduced interval of the remaining design variables. Since the projection considers the complete solution box, a change in the permissible intervals of the remaining design variables does have an effect on the projection. Hence, this projection technique is a powerful support for design space exploration [13]. The software `ClearVU Solution Space` (version 2.2.22) is used for the SSE analysis.

3. Application

The proposed workflow in the previous section was applied to the mount stiffnesses of the double decoupled mounting system presented in Section 2.1.

3.1. Problem Definition

The first step was to define design variables as well as their design spaces. Instead of varying all eight mounts independently of each other, we reduced the system complexity by using symmetry of the mounting topology according to the reference system, which has three types of mounts mirrored along the y-axis. This results in a nine-dimensional design space. In Table 1, the lower bound and upper bound of the design space for each design variable are listed. To consider the continuum resonances of mounts, we set up the upper bound by a minimum factor two larger than the lower bound. From field experience, the overall limit of these mount types was defined as 2.5 $\frac{\mathrm{kN}}{\mathrm{mm}}$. For reasons of completeness, the rear inner mounts are listed separately to emphasize the changes in direction due to the 90° rotation. This means that a modification of the x stiffness impacts not only the x but also the y-direction of the entire system.

Table 1. Design space for mount stiffness values.

Mount Name	Design Space $[\frac{\mathrm{kN}}{\mathrm{mm}}]$	
	Lower Bound [x y z]	**Upper Bound [x y z]**
Front inner mount (inM)	[0.25, 0.50, 1.25]	[1.0, 2.00, 2.5]
Rear inner mount (inM)	[0.50, 0.25, 1.25]	[2.0, 1.00, 2.5]
Front outer mount (foM)	[0.20, 0.06, 0.25]	[0.8, 0.32, 1.0]
Rear outer mount (roM)	[0.20, 0.10, 0.22]	[1.0, 0.48, 1.1]

The training data for the data-driven models were generated using the superelement technique, improving the simulation time by a factor of 10. The main advantage is that the dynamic behavior of the unmodified substructure only needs to be calculated once. This enables an efficient reuse in follow-up analysis cycles or large designs of experi-

ments (DoEs) [22] of high-dimensional systems. Figure 4 shows the skyline of the SPL over the frequency range of 250 to 1500 Hz for the ear position at the driver's seat, generated by 1000 sample points. The calculation is based on the hybrid simulation technique, multiplying the simulated mount forces with the vehicle transfer functions into the cabin, as presented in Section 2.3. The skyline plot shows a SPL scatter band of approximately 20 dBA. For the sake of simplicity, a constant dashed target line f_c is introduced, representing the system requirement, and can be interpreted as a simplified perception threshold for the structure-borne noise through the mounts. Considering additional transmission paths or road-induced masking effects may necessitate a modified target line, which can be a curve of any form depending on the specific application. Ideally, the SPL should remain below this threshold. This is the case for a broad frequency range, such as above 1 kHz. However, in the narrow frequency band around 800 Hz, there is no combination of mount stiffnesses that meets this target, meaning that this threshold is not achievable.

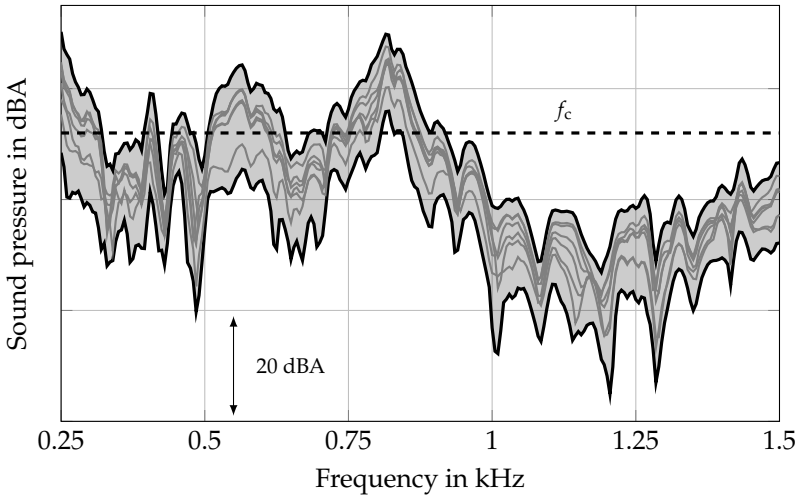


Figure 4. Skyline plot of the SPL at the driver's seat for the sampled mount stiffnesses, based on the design space defined in Table 1, with a constant threshold curve f_c.

The performance of the NN presented in Section 2.4 is depicted in Figure 5 in the form of MSE for training data (solid) as well as test data (dashed-dot) over epochs and coefficient of determination of the latter. Besides the 1000 training data points, we applied 200 randomly generated testing data points within the design space to evaluate prediction performance on unseen data.

While the losses decrease similarly up to 10^2 epochs, the testing loss begins to drop down more smoothly and takes the form of an asymptotic behavior. No overfitting characteristics are identifiable during this training phase. Moreover, the coefficient of determination $R^2 = 0.9957$ is close to $R^2 = 1$, indicating a more than adequate correlation between actual values and predicted values.

The numerical efficiency of the physical model and the data-driven model was evaluated based on the average computational time for a single simulation run. Simulations were conducted under identical conditions. The data-driven model (0.016 s) outperformed the FEM model (114 s) by a factor of approximately $7.19 \cdot 10^3$. Moreover, increasing the number of simulation runs to 1000 raised the total runtime of the data-driven model to 0.04 s, demonstrating its feasibility for the SSE approach. Performing the same number of FEM simulations would take hours or even days and would also be limited by the available hardware.

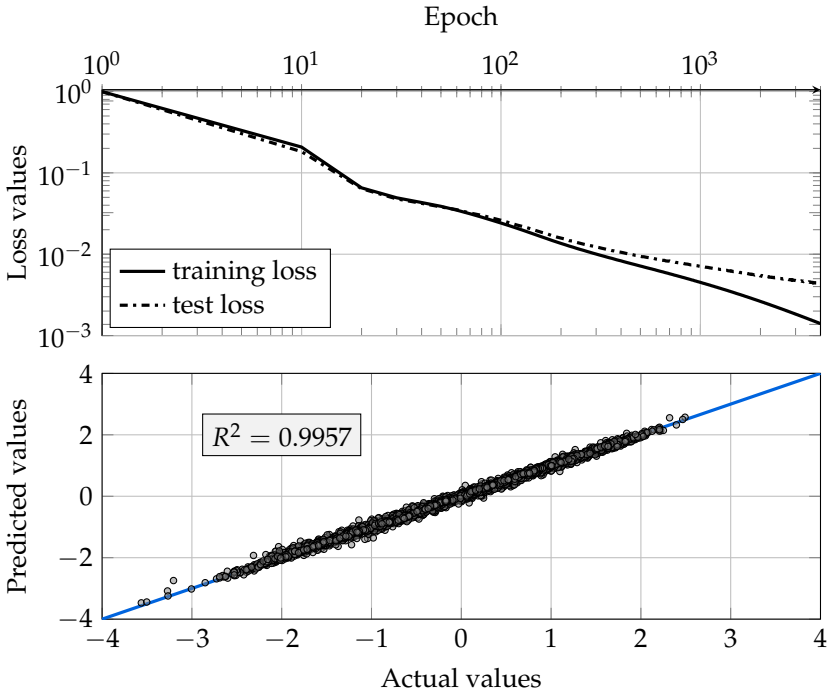


Figure 5. Performance of the NN evaluated using MSE over epochs and the coefficient of determination.

3.2. Identification of Frequency-Dependent Solution Box

The procedure for identifying a frequency-dependent solution box is to concatenate the solution box of each frequency point, enabling smooth permissible stiffness curves. For the sake of simplicity, we propose discretizing the frequency range into equidistant frequency bands $f_{\mathrm{b},i}$ with a step size of 50 Hz and taking the maximum value of the SPL within this range.

We start with the first frequency band $f_{\mathrm{b},1}$ by first optimizing for the best design, followed by a solution box optimization seeking the largest volume. The solution box optimization provided by `CVSS` is based on the proposed Monte Carlo optimization algorithm by [16], generating a initial candidate solution box after a predefined number of iterations. Afterwards, the solution box is revised and if necessary, manually expanded by exploring the design space using box projections. In our application example, the proposed solution boxes often do not cover the borders of the design space accurately enough, which results in a manual expansion.

The solution box plots are composed of nine projection plots ordered in a matrix form, where the first row corresponds to the inner mount and the second as well as the third row represent the outer mounts. Due to the odd number of design variables in this application, a design variable has to be plotted twice to fill out the missing pairing partner. The axes of each projection plot correspond to a design variables defined in Table 1. The solution box plots are visualized as described in Section 2.5, where green colored regions indicate that all requirements are fulfilled, while red areas show that at least one requirement is violated. The solution box is depicted as black solid rectangles.

The solution box projection of the first frequency band is depicted in Figure 6. It is clearly noticeable that the design variables, besides the z-directions, do not have any limitations. This is visualized by fully green areas, meaning that the design space of these variables is equal to the solution box interval. Physically, this means that main structure-borne noise path is dominated by the z-direction of each mount. The most restricted stiffness variables, in terms of the relation of permissible range and design space, are represented by the roM, followed by the inner mounts and the foM.

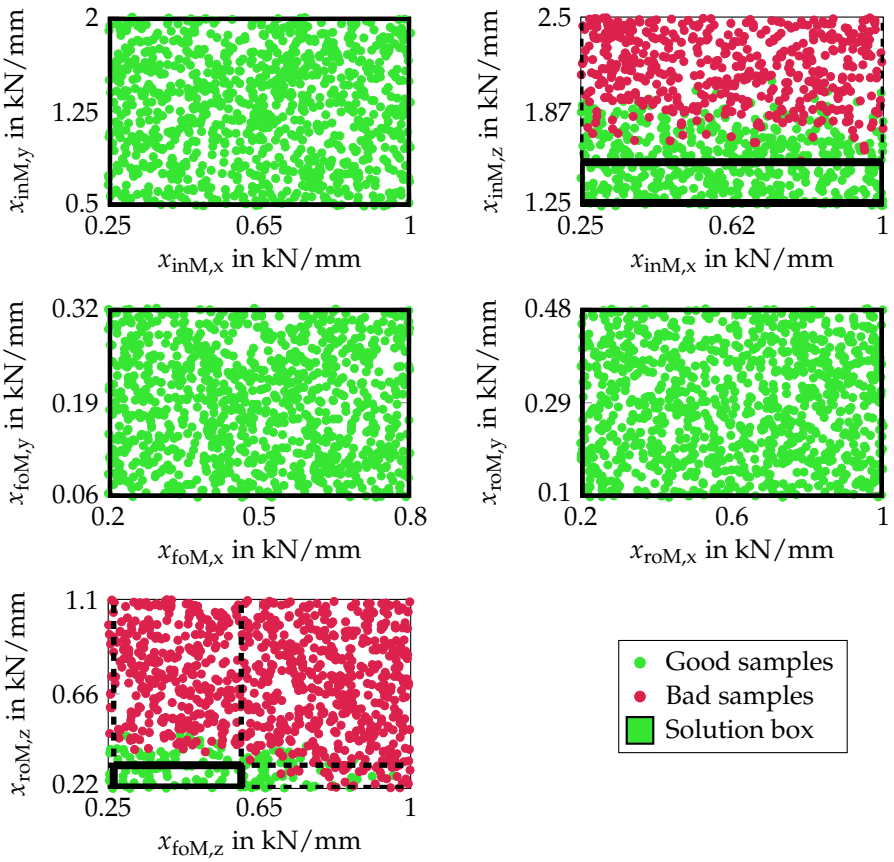


Figure 6. Projection plot of the solution box for all mount stiffness values for the frequency band $f_{\mathrm{b},1}$ (250 to 300 Hz).

For the frequency bands $f_{\mathrm{b},i}$ with $i \geq 2$, the solution box of the previous frequency band $f_{\mathrm{b},i-1}$ is used as initial condition to ensure continuity of the solution space used in this study. An alternative strategy could be to run the same procedure as for the first frequency band. This is valid as long as the solution spaces are connected. Otherwise, there could be some cases where the solution spaces are not attached to each other or the suggested solution box from optimization does not represent the best solution in terms of practicability. An example of this is shown in Figure 7, where the solution box projection of the z stiffnesses for the inner and rear outer mounts is depicted. The remaining variables are not visualized because they are not restricted regarding design space. The plot shows different solution boxes, where box number one represents the proposed best solution from optimization. This box is characterized by the enlargement of the variable $x_{\mathrm{inM},z}$ and the simultaneous restriction of the opposing variable $x_{\mathrm{roM},z}$. Here, a physical understanding of the mount design is crucial and is not taken into account by the optimizer. The inner mounts x_{inM} of the considered mounting system are stiffer than the outer mounts x_{roM}, which leads to continuum resonances of the mount at high frequency ranges. Therefore, the resonance of the softer mounts within the lower frequency bands is expected. Rather than restricting the softer mount type, we manually adjusted the solution box, considering the physical properties of the softer mount while accepting some loss of the solution box. The second box, depicted in Figure 7, represents an exemplary manually adjusted solution box, demonstrating the methodology's capacity to generate a range of feasible solution boxes.

As already explained in the previous section, the SSE analysis confirms the absence of a solution box within the frequency band between 800 and 850 Hz. Therefore, the structural weakness with respect to the structure-borne noise path through mounts cannot be compensated by any combination of mount properties. In order to reach targets, additional measures

such as reducing the primary excitation or improving the transfer path by stiffening the structural environment have to be introduced. Furthermore, especially in these regions, it is important to avoid resonance effects of the mounts. By relaxing the target value, one can nevertheless identify the potential in the form of a solution box for the mounts, which is depicted in Figure 8. Here, the solution box projection for the frequency band between 800 and 850 Hz for a modified target curve is shown. The adjusted target value for this frequency band is locally relaxed by 40%, resulting in $f_{c,mod} = 1.4 f_c$. Consequently, the overall target line is no longer constant. In comparison to the first frequency band, nearly all design variables are restricted regarding their design space, except for the inner mount in the y-direction. In particular, the x-direction behaves similarly to the z-direction with respect to their permissible intervals, indicating an additional relevant transfer path in this frequency band.

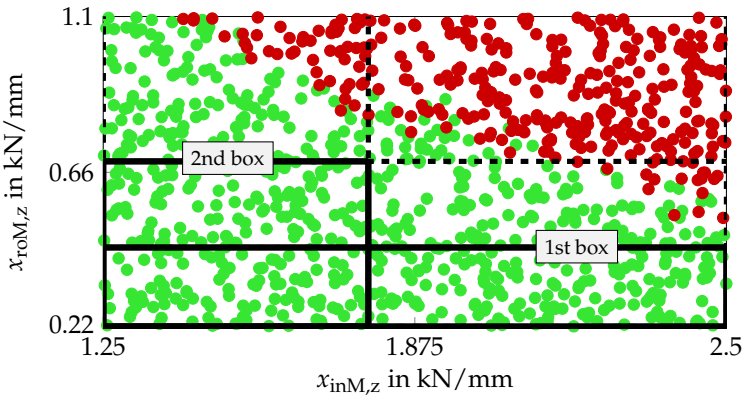


Figure 7. Projection plot of two different solution boxes of the mount stiffnesses $x_{inM,z}$ and $x_{roM,z}$ in the frequency band $f_{b,2}$ (300 to 350 Hz). Green dots indicate good samples; red dots indicate bad samples.

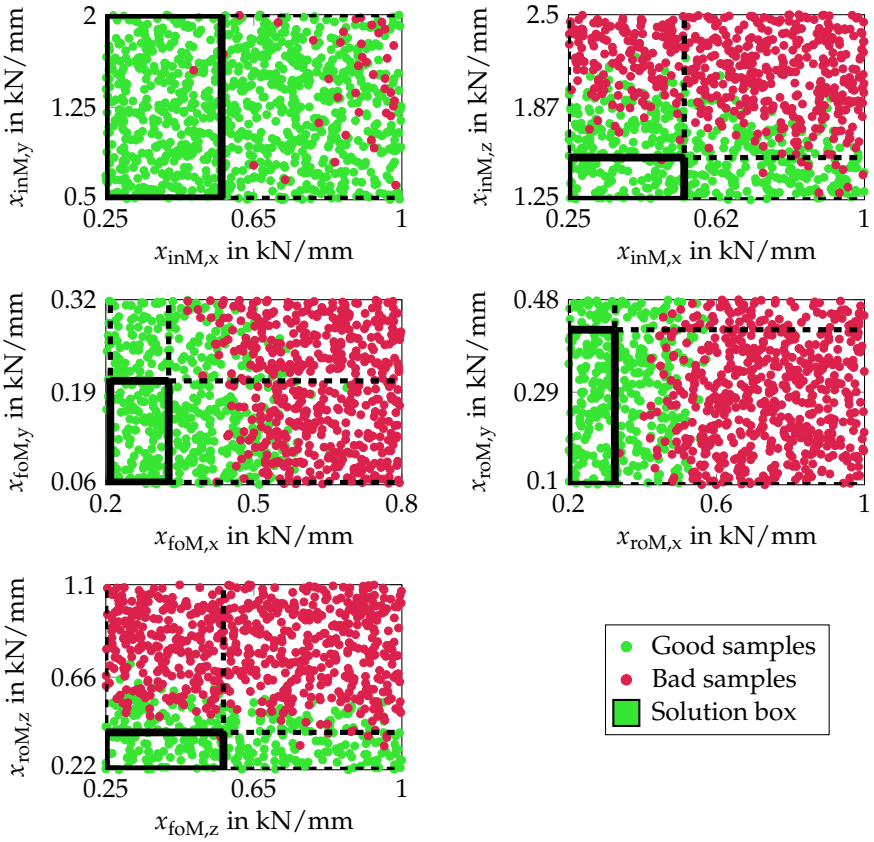


Figure 8. Projection plot of the solution box for all mount stiffness values in the frequency band $f_{b,12}$ (800 to 850 Hz) with the adjusted target curve $f_{c,mod}$.

The procedure for generating solution boxes is performed for all frequency ranges. By allocating the permissible intervals of each design variable over the frequency, we are able to generate a robust frequency-dependent stiffness range within the system to ensure that the requirements are fulfilled. This is exemplarily performed for the rear outer mount in all directions; see Figure 9. As in the projection plots, the green areas represent the permissible regions, and within the red areas the formulated requirements are violated. Except for the frequency band $f_{b,12}$, all solution boxes are generated by fulfilling the target value c_f. Furthermore, it can be observed that the impact of the x- and z-directions varies across different frequency ranges. But all directions show a small solution box around 800 Hz due to the dominant contribution of the mounts. Above 1000 Hz all stiffnesses within the design space reach the target, which was expected from the skyline plot. This means that the structure-borne noise contribution of the mounts is no longer dominant. This aligns with field experience, where structure-borne noise contribution commonly decreases while the airborne-noise increases at higher frequencies.

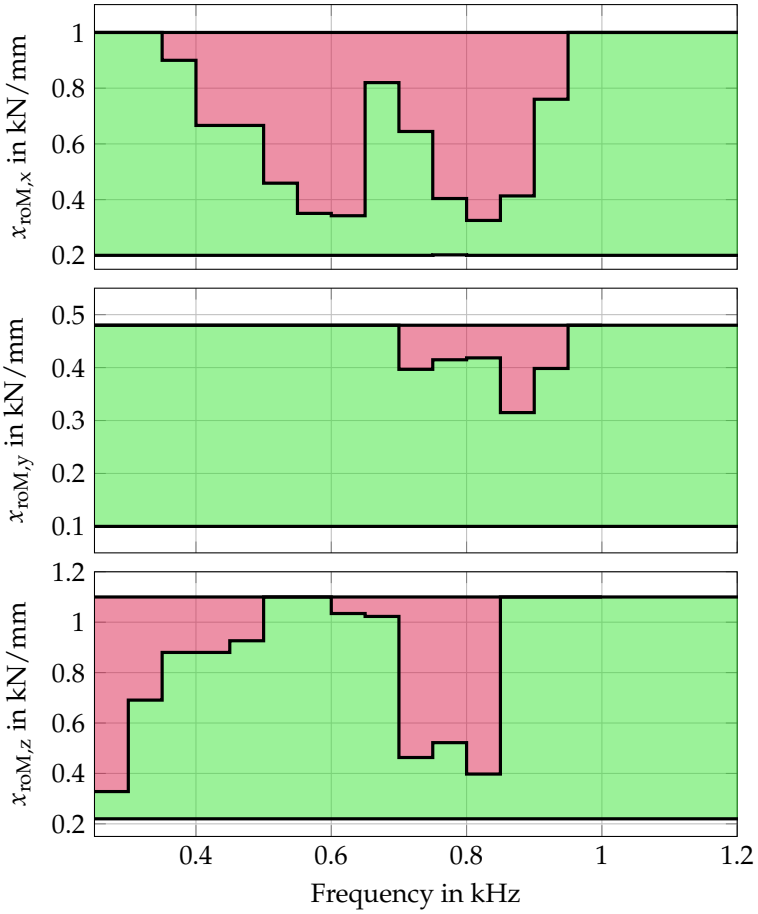


Figure 9. Frequency-dependent permissible interval of the rear outer mount in all directions, obtained by concatenating the intervals of each frequency band $f_{b,i}$, shown as green areas.

These generated permissible intervals of a mount can be used during mount development. These intervals provide more precise information regarding the ideal placement of continuum resonances or where they should be avoided. Especially for some critical frequency ranges, determined by large excitation of the EDU or structural weaknesses, this approach provides a guideline for mount design. Any stiffness curve within the green area will fulfill the system requirements. Moreover, these design variables are decoupled from each other. Each design variable can vary within its permissible range independently of all other design variables while fulfilling all the determined NVH requirements. This

methodology can be further extended to other development disciplines, such as vehicle dynamics and durability, in order to identify common solution spaces.

4. Conclusions and Outlook

In this work, we present an approach to identify robust noise, vibration and harshness (NVH) requirements regarding dynamic stiffness at the component level of engine mounts while fulfilling system targets over a frequency range up to 1500 Hz. An integral part of the workflow is the set-based design approach solution space engineering (SSE). Instead of searching for an optimal dynamic stiffness curve, we seek frequency-dependent permissible intervals of each stiffness value, while maintaining the decoupling of these design parameters. By extending the concept of generating a solution box for a specific frequency point or range, we are able to identify frequency-dependent permissible intervals over the frequency range of interest by concatenating these solution boxes. The data-driven modeling technique plays an important role in this context by drastically reducing the simulation time of highly accurate finite-element models by a factor of $7.19 \cdot 10^3$, thereby enabling a large number of simulation variants, which is mandatory for the SSE analysis. This kind of approach provides a more precise requirement definition at the component level, such as the ideal location of mount continuum resonances, while at the same time providing major flexibility given by permissible intervals of the dynamic stiffnesses. This tailored requirement can be used during the development of engine mounts, especially for the evaluation of NVH properties of engine mounts. Any dynamic stiffness characteristic of a proposed mount concept, realized during the design process and lying within the derived permissible interval, will achieve the predefined target. Moreover, it enables the consideration of uncertain data, especially during the early design phase of development and later changes in design.

For future research, phase information of engine mounts will be included in the proposed design procedure in order to describe more precisely the entire mount behavior, which can be more complex in the sense of an increasing number of design variables. Consequently, other disciplines, such as durability or vehicle dynamics, along with variations in seat position, must be considered as target requirements, potentially reducing the solution box. Furthermore, structural properties of the surrounding components besides the powertrain mounting system, such as material properties or component morphing, can be integrated by seeking an integrative development and exploring the potentials of both subsystems. Considering the remaining structure-borne paths, such as through side shafts, the contribution of these transmission paths to the interior cabin must be quantified via transfer path analysis before deriving the solution space for the mounts. Potential readjustments of the target curve must also be evaluated. By increasing the number of design variables, different machine learning approaches for data-driven modeling should be considered and benchmarked in terms of performance and applicability during the development process.

Author Contributions: Conceptualization, J.G.C.L. and S.H.; methodology, J.G.C.L.; software, J.G.C.L.; validation, J.G.C.L., S.H. and K.F.; formal analysis, J.G.C.L.; investigation, J.G.C.L.; data curation, J.G.C.L.; writing—original draft preparation, J.G.C.L.; writing—review and editing, K.F. and S.H.; visualization, J.G.C.L.; supervision, K.F. and S.H.; project administration, J.G.C.L. All authors have read and agreed to the published version of the manuscript.

Funding: This research received no external funding.

Data Availability Statement: The data presented in this study are available on request from the corresponding author due to restrictions related to internal company confidentiality.

Acknowledgments: The authors thank Mercedes-Benz AG, particularly the NVH Powertrain department and the NVH Powertrain Integration team member, for their support and for always being available to discuss the ongoing research. Additionally, the authors would like to thank the Fraunhofer Institute for Structural Durability and System Reliability LBF for their valuable input and support.

Conflicts of Interest: Author José Cóndor López and Karsten Finger are employed by the company Mercedes-Benz AG. The remaining authors declare that the research was conducted in the absence of any commercial or financial relationships that could be construed as potential conflicts of interest.

Abbreviations

The following abbreviations are used in this manuscript:

NVH	Noise, vibration and harshness
BEV	Battery electric vehicle
PMS	Powertrain mounting system
SSE	Solution space engineering
EDU	Electric drive unit
inM	Inner mount
foM	Front outer mount
roM	Rear outer mount
SPL	Sound pressure level
NN	Neural Network
FE	Finite element
MSE	Mean squared error

References

1. Lieske, D.; Landes, D.; Fischer, J. Optimization of thePowertrain Noise for the Electric Vehicle Mercedes-Benz EQC. *ATZ Worldw.* **2020**, *122*, 60–64. [CrossRef]
2. Droste, M.; Rieß, S.; Cóndor López, J.; Erraji, A. Vibroacoustic Metamaterials for Reduced Sound Radiation of an Electric Powertrain. *MTZ Worldw.* **2023**, *84*, 44–47. [CrossRef]
3. Wellmann, T.; Tousignant, T.; Govindswamy, K.; Tomazic, D.; Steffens, C.; Janssen, P. NVH Aspects of Electric Drive Unit Development and Vehicle Integration. In Proceedings of the Noise and Vibration Conference & Exhibition, Grand Rapids, MI, USA, 10–13 June 2019; SAE International: Warrendale, PA, USA, 2019. [CrossRef]
4. Steffens, C.; Lechner, C.; Lauen, M.; Suresh, H. Challenges for Vehicle NVH and Acoustics Due to Electric Mobility. *ATZ Worldw.* **2023**, *125*, 38–43. [CrossRef]
5. GmbH, U. eMobility Fahrzeug-Studie 2021, 2021. Available online: https://www.p3-group.com/p3-updates/p3-charging-index-2024/#:~:text=Der%20P3%20Charging%20Index%20wurde,reale%20Reichweite%20in%20Kilometern%20nachzuladen (accessed on 16 September 2025)
6. Blickensdorff, J.; Boulliung, M.; Burkard, M.; Dold, C.; Emretsson, B.G.; Genuit, K.; Graf, B.; Kurch, M.; Millithaler, P.; Mohr, C.; et al. Akustik. In *Elektrifizierung des Antriebsstrangs: Grundlagen-vom Mikro-Hybrid zum Vollelektrischen Antrieb*; Tschöke, H., Gutzmer, P., Pfund, T., Eds.; Springer: Berlin/Heidelberg, Germany, 2019; pp. 307–363. [CrossRef]
7. Münder, M.; Carbon, C.C. A literature review [2000–2022] on vehicle acoustics: Investigations on perceptual parameters of interior soundscapes in electrified vehicles. *Front. Mech. Eng.* **2022**, *8*, 974464. [CrossRef]
8. Nataraja S, M.; Rao, M.; Raghavendran, P.; Selvam, E. NVH Refinement of Structure-Borne Tonal Noise in Electric Vehicle. In Proceedings of the Symposium on International Automotive Technology, Pune, India, 23–25 January 2024; SAE International: Warrendale, PA, USA, 2024. [CrossRef]
9. Gröne, M.; Schwarzendahl, S.; Troge, J.; Hensel, E. Transfer Stiffness Characterization of Elastomer Mounts at High Frequencies. *ATZ Worldw.* **2025**, *127*, 40–43. [CrossRef]
10. Kruse, E.; Sell, H.; Loecken, F. Electric Motor Mounting System Validation with Subsystem and Powered e-Axle Tests. In Proceedings of the Noise and Vibration Conference & Exhibition, Grand Rapids, MI, USA, 15–18 May 2023; SAE International, Warrendale, PA, USA, 2023.
11. Bahr, S.; Jacobs, G.; Höpfner, G.; Hensel, E.; Troge, J.; Rapp, T. Topology optimization of nonlinear elastomer engine mounts considering the transfer behavior. *Forsch. Ingenieurwesen* **2025**, *89*, 72. [CrossRef]

12. Stoll, G.; Atzrodt, H.; Hansen, T.; Hülsebrock, M.; Kleinfeller, N. Application of vibroacoustic metamaterial to compensate continuum resonance in powertrain mounting systems for electric vehicles. In Proceedings of the 2024 Eighteenth International Congress on Artificial Materials for Novel Wave Phenomena (Metamaterials), Chania, Greece, 9–14 September 2024; pp. 1–3. [CrossRef]
13. Cóndor López, J.; Stumpf, J.; Freitag, H.G. Robust design optimization of nonlinear powertrain mounting systems with solution space engineering. In Proceedings of the International Conference on Noise and Vibration Engineering (ISMA 2022) and International Conference on Uncertainty in Structural Dynamics (USD 2022), Leuven, Belgium, 12–14 September 2022.
14. Grimm, A.; Finger, K.; Stoll, G.; Atzrodt, H.; Herold, S. Implementation of a modular model for active engine mounts and coupling with a reduced model for full-vehicle NVH-simulation. In Proceedings of the Aachen Acoustics Colloquium 2018, Aachen, Germany, 26–28 November 2018; pp. 93–102.
15. Qureshi, A.J.; Dantan, J.Y.; Bruyere, J.; Bigot, R. Set-based design of mechanical systems with design robustness integrated. *Int. J. Prod. Dev.* **2014**, *19*, 64–89. [CrossRef]
16. Zimmermann, M.; von Hoessle, J.E. Computing solution spaces for robust design. *Int. J. Numer. Methods Eng.* **2013**, *94*, 290–307. [CrossRef]
17. Königs, S.; Zimmermann, M. Resolving conflicts of goals in complex design processes—Application to the design of engine mount systems. In Proceedings of the 7th International Munich Chassis Symposium Munich, Germany, 14–15 June 2016; Pfeffer, P., Ed.; Springer Vieweg: Wiesbaden, Germany, 2017; pp. 125–141.
18. Xu, D. Vibration and Noise Reduction Using Solution Spaces. Ph.D. Thesis, Technical University of Munich, Munich, Germany, 2024.
19. Xu, D.; Häußler, M.; Zimmermann, M. Requirement Definition for a Vibration Source Using Transfer Path Analysis and Solution Spaces. In Proceedings of the Automotive Acoustics Conference 2023, Rueschlikon, Switzerland, 11–12 July 2023; Heintzel, A., Ed.; Springer Vieweg: Wiesbaden, Germany, 2025; pp. 53–68.
20. Horváth, K.; Zelei, A. Simulating Noise, Vibration, and Harshness Advances in Electric Vehicle Powertrains: Strategies and Challenges. *World Electr. Veh. J.* **2024**, *15*, 367. [CrossRef]
21. Zeller, P. (Ed.) *Handbuch Fahrzeugakustik: Grundlagen, Auslegung, Berechnung, Versuch*; Springer Vieweg: Wiesbaden, Germany, 2018. [CrossRef]
22. Fiedler, U.; Visser, R.; Kreissig, V. Interior noise optimization of powertrain induced vibrations for an electric vehicle using machine learning methods. In Proceedings of the Automotive Acoustics Conference, Rueschlikon, Switzerland, 11–12 July 2023.
23. Cóndor López, J.; Hansen, T.; Weber, A.; Kleinfeller, N.; Finger, K. Gezielte Modifikation des Übertragungsverhaltens von Elastomerlagern durch den Einsatz von vibro-akustischen Metamaterialien. In Proceedings of the Fortschritte der Akustik—DAGA 2024, Hannover, Germany, 18–21 March 2024.
24. Hornik, K.; Stinchcombe, M.; White, H. Multilayer feedforward networks are universal approximators. *Neural Netw.* **1989**, *2*, 359–366. [CrossRef]
25. Hughes, A.; Grawoig, D. *Statistics, a Foundation for Analysis*; Business and Economics Series; Addison-Wesley Publishing Company: Boston, MA, USA, 1971.
26. Stumpf, J.; Naumann, T.; Vogt, M.; Duddeck, F.; Zimmermann, M. On the Treatment of Equality Constraints in Mechanical Systems Design Subject to Uncertainty. In Proceedings of the NordDesign 2020, Lyngby, Denmark, 12–14 August 2020. [CrossRef]
27. Zimmermann, M.; Königs, S.; Niemeyer, C.; Fender, J.; Zeherbauer, C.; Vitale, R.; Wahle, M. On the design of large systems subject to uncertainty. *J. Eng. Des.* **2017**, *28*, 233–254. [CrossRef]

Disclaimer/Publisher's Note: The statements, opinions and data contained in all publications are solely those of the individual author(s) and contributor(s) and not of MDPI and/or the editor(s). MDPI and/or the editor(s) disclaim responsibility for any injury to people or property resulting from any ideas, methods, instructions or products referred to in the content.